

# Generating an effective magnetic lattice for cold atoms

Xinyu Luo,<sup>1,2,3</sup> Lingna Wu,<sup>1,3</sup> Jiyao Chen,<sup>1,3</sup> Rong Lu,<sup>1,3</sup> Ruquan Wang,<sup>2,3</sup> and L. You<sup>1,3</sup>

<sup>1</sup>*State Key Laboratory of Low Dimensional Quantum Physics,*

*Department of Physics, Tsinghua University, Beijing 100084, China*

<sup>2</sup>*Institute of Physics, Chinese Academy of Sciences, Beijing 100080, China*

<sup>3</sup>*Collaborative Innovation Center of Quantum Matter, Beijing, China*

(Dated: October 8, 2018)

We present a general scheme for synthesizing a spatially periodic magnetic field, or a magnetic lattice (ML), for ultracold atoms using pulsed gradient magnetic fields. Both the period and the depth of the artificial ML can be tuned, immune to atomic spontaneous emission often encountered in optical lattices. The effective Hamiltonian for our 2-dimensional ML has not been discussed previously in condensed matter physics. Its band structures show interesting features which can support topologically nontrivial phases. The technical requirements for implementing our protocol are readily available in today's cold atom experiments. Realization of our proposal will significantly expand the repertoire for quantum simulation with ultracold atoms.

PACS numbers: 67.85.Jk, 03.75.Mn, 03.75.Ss, 37.10.Jk

Optical lattice (OL) is a highly controllable environment where many body physics can be studied with ultracold atoms [1, 2]. Additionally, atoms in OL promise exciting opportunities in quantum information science [3–5]. Many lattice geometries have been realized experimentally, from 3-dimensional (3D) cubic lattices [6] to honeycomb lattices [7] and kagome lattices [8]. With spin-dependent OLs, atomic internal degrees of freedom such as its spin or pseudo-spin, are coupled to its spatial degrees of freedom. This can give rise to interesting phenomena [9–18], absent in spin-independent lattices. For example, attractive Fermi gases in one-dimensional (1D) lattices support three-body bound states with only two-body interactions when the tunneling rates are spin-dependent [19]. In 3-dimension, recent theoretical studies predict a exotic state with the coexistence of superfluid and normal components [20]. For bosons, recent experiments reveal a new phase in spin-dependent OLs, with one spin component Mott-insulating and the other superfluid. The superfluid to Mott-insulating transition is modulated by their mutual interactions [21].

A topical area of intense research interest in ultracold atoms concerns synthetic gauge fields [22]. Several theoretical studies have proposed ideas to synthesize artificial gauge potentials for atoms (with hyperfine spin  $F$ ) in OL systems [23–27], many starting with simple forms  $\propto F_z$  or spin-dependent lattices and periodically driving the systems [28–30]. Some of the ideas are realized in recent experiments [31, 32]. They emulate atomic interactions with synthetic magnetic fields or spin-orbit coupling (SOC). Additional interactions are therefore required to flip atomic spins in order to broaden the scope of quantum simulations. More general spin-dependent lattices and artificial gauge fields can support exotic quantum phases [33–37]. For example, W. Hofstadter *et al.* [33] find fermionic systems exhibit quantum phases such as topological and normal insulator, metal, or semi-metal, all with two or more Dirac cones even in the absence of atomic interactions when a staggered potential is added

to an artificial Rashba-type SOC. In the presence of strong atomic interactions, semi-metal to antiferromagnetic insulator transition can occur.

Spin-dependent OL can be readily generated by light shifts with spin-dependent modulations [38], as in the familiar lin- $\theta$ -lin setup [12, 39]. 1D effective Zeeman lattice can be produced by combining a radio-frequency (RF) magnetic field with Raman laser fields [40]. However, due to the same scaling with laser intensity and detuning, the ratio of spontaneous emission rate to the spin dependent lattice depth is determined by the ratio of atomic natural linewidth to its excite state fine structure splitting. The resulting spin dependent lattice depth thus will be small in order to suppress spontaneous emission [41–43]. Furthermore, the ideas based on light-atom interaction are limited by the laser wavelength, which make the spatial periods of the resulting OLs difficult to tune. Larger spacing spin dependent lattice potentials can be realized through microfabricated wires or permanent magnet arrays on an atom chip [44–46].

This work presents a different approach for synthesizing a spatially periodic magnetic field or a magnetic lattice (ML) using pulsed gradient magnetic fields. It can be understood in terms of spatial dependent spin rotations, which couple atomic internal degrees of freedom with its spatial/orbital degrees of freedom. While sharing some features with the earlier mechanism for SOC [47] and an analogous scheme using zero average modulated gradient magnetic fields [48], the present idea opens the door towards a class of synthesized ML not previously explored. It can be implemented by introducing a bias magnetic field to the free evolution part of the SOC protocol [47]. The ML lattice constant is tunable and can overcome the laser wavelength limit. Furthermore, the scheme we present can be generalized in a straightforward manner to more than one spatial dimension.

This Letter is organized as follows. First, our idea for synthesizing a ML with a bias magnetic field during the free evolution period of the SOC protocol [47]

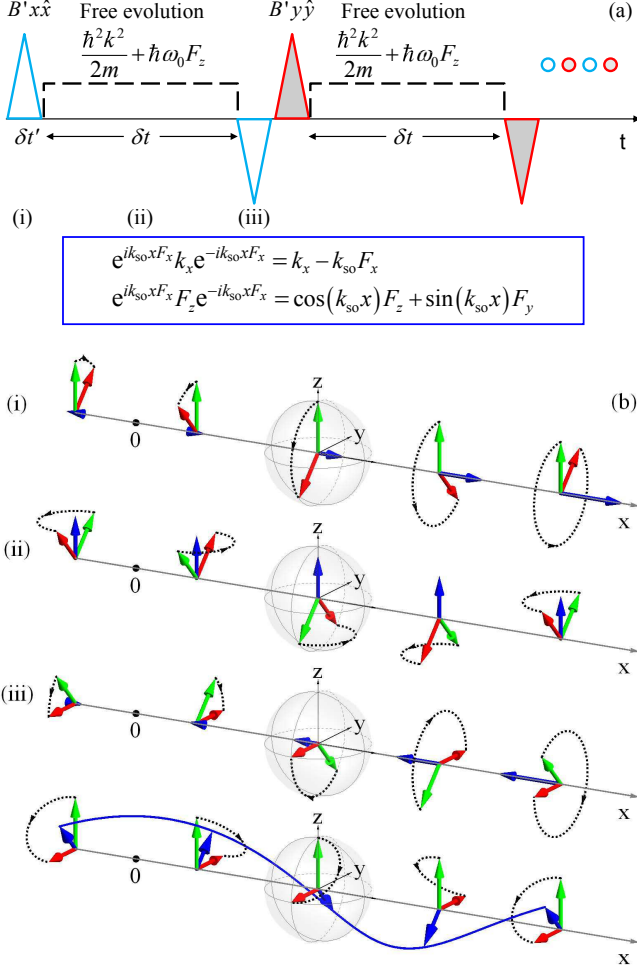


FIG. 1: (a) A single period of our protocol starting with free evolution in a bias field (in black dashed line) sandwiched in between a  $x$ -gradient pulse pair (in blue solid lines), followed by an analogous  $y$ -gradient pulse pair (in red solid lines). The opposite pulse pair affects unitary transformations as displayed inside the rectangular box; (b) Spatial dependent spin rotations are illustrated for atoms located along the  $x$ -axis. Each row refers to a different temporal instant marked in (a): (i) [(iii)] at the first [second]  $x$ -gradient pulse, affects clockwise [counter-clockwise] spin rotations around the  $x$ -axis, while free evolution in the  $z$ -bias field is shown in (ii). In (i), (ii), and (iii), green, red, and blue arrows denote respectively the initial, the final spin directions, and the local magnetic fields. The last row shows the synthesized ML (blue arrows), which is equivalent to have spins rotated from the initial directions (green arrows) to the final directions (red arrows). The envelope for the ML is outlined in thick blue line.

is introduced. The dynamics governed by the synthesized Hamiltonian are analyzed and numerically simulated, which support our claim that the protocol we present is valid and effective. The band structures for our ML are then computed. We discuss conditions and signatures for experimentally synthesizing and testing our ML. Finally we summarize and discuss several potential

experimental challenges for implementing our idea.

Our idea for generating a 2-dimensional (2D) ML can be most easily appreciated in comparison to the earlier SOC protocol using gradient magnetic field pulses [47]. As is illustrated in Fig. 1(a) for one period, the first (second) half is composed of free evolution in a uniform magnetic field  $B_0 \hat{z}$ , sandwiched in between two short  $x$ - ( $y$ -) gradient magnetic field pulses  $B' x \hat{x}$  ( $B' y \hat{y}$ ) with opposite amplitudes.  $B'$  denotes the averaged first order spatial derivative, or the spatial gradient, of the magnetic field.  $\delta t'$  denotes the duration of each pulse, which is assumed small and the same for all pulses, while  $\delta t$  is the duration between the two pulses.  $T/2 = \delta t$  is half the period. Extending the SOC protocol [47], a nonzero bias magnetic field along  $z$ -direction gives rise to the 2D ML.

The dynamics from the first pulse are simple, with its evolution operator given approximately by  $U_x(\delta t') = \exp(-ig_F \mu_B B' x F_x \delta t' / \hbar)$ , only due to the averaged Zeeman term  $g_F \mu_B B' x F_x$ , which is assumed to overwhelm all other interactions.  $\mu_B$  is the Bohr magneton.  $g_F$  is the Lande  $g$ -factor for the  $F = 1$  ground state Zeeman manifold considered.  $F_{x,y,z}$  denotes the  $x$ -,  $y$ -, and  $z$ -component of  $\vec{F}$ . The pair of  $x$ -gradient pulses give

$$\begin{aligned} U_x(T/2, 0) &= U_x(\delta t') \exp(-iH_0 \delta t / \hbar) U_x^\dagger(\delta t') \\ &= \exp(-iH_{\text{eff}}^{(x)} \delta t / \hbar), \end{aligned} \quad (1)$$

which transforms the free evolution Hamiltonian  $H_0 = \hbar^2 k^2 / (2m) + \hbar \omega_0 F_z$  into a SOC plus a ML

$$\begin{aligned} H_{\text{eff}}^{(x)} &= \frac{\hbar^2}{2m} \left[ (k_x - k_{\text{so}} F_x)^2 + k_y^2 \right] + \\ &\quad \hbar \omega_0 \left[ \cos(k_{\text{so}} x) F_z + \sin(k_{\text{so}} x) F_y \right], \end{aligned} \quad (2)$$

where  $\omega_0 = g_F \mu_B B_0 / \hbar$  is the Larmor frequency at  $B_0$ . The first line of Eq. (2) corresponds to SOC [47], whose strength is given by the momentum impulse  $\hbar k_{\text{so}} = g_F \mu_B B' \delta t'$  from the gradient pulse [47]. The second line corresponds to a ML  $\propto \sin(k_{\text{so}} x) \hat{y} + \cos(k_{\text{so}} x) \hat{z}$  with wave vector  $k_{\text{so}}$  as illustrated in Fig. 1(b). Follow up with a pair of  $y$ -gradient pulses as shown in Fig. 1(a), we end up with the two dimensional (2D) version

$$U_{2D}(T, 0) = U_y(T, T/2) U_x(T/2, 0) \approx \exp(-iH_{\text{eff}}^{(2D)} T / \hbar),$$

with

$$\begin{aligned} H_{\text{eff}}^{(2D)} &= \frac{\hbar^2}{2m} (k_x - \frac{1}{2} k_{\text{so}} F_x)^2 + \frac{\hbar^2 k_{\text{so}}^2}{8m} F_x^2 + \\ &\quad \frac{\hbar^2}{2m} (k_y - \frac{1}{2} k_{\text{so}} F_y)^2 + \frac{\hbar^2 k_{\text{so}}^2}{8m} F_y^2 + \\ &\quad \frac{1}{2} \hbar \omega_0 [F_z \cos(k_{\text{so}} x) + F_y \sin(k_{\text{so}} x)] + \\ &\quad \frac{1}{2} \hbar \omega_0 [F_z \cos(k_{\text{so}} y) - F_x \sin(k_{\text{so}} y)], \end{aligned} \quad (3)$$

provided the effective action from each cycle is small such that we can use Trotter expansion to the first order and combine the non-commuting  $x$ - and  $y$ -dependent

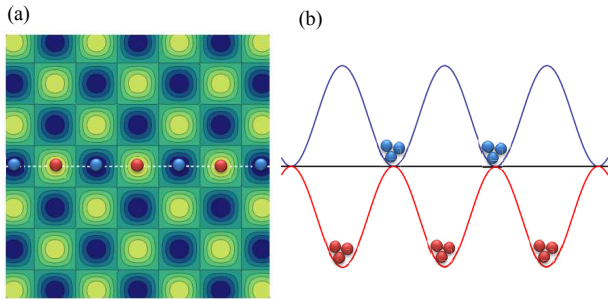


FIG. 2: (a) Internal state dependent lattice potentials for atoms in the 2D ML; (b) A 1D cut along the dashed line in (a). The blue and red lines denote  $M_F = 1$  and  $-1$  states, respectively. The magnetic field insensitive  $M_F = 0$  state is denoted by the straight black line.

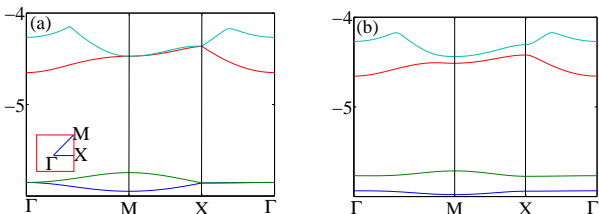


FIG. 3: Single particle energy spectrum (in units of  $\hbar\omega_R$ ) for the lowest four bands, plotted for a contour in the first Brillouin zone, as shown by the (red square) insert, connecting reciprocal momentum points along  $\Gamma \rightarrow M \rightarrow X \rightarrow \Gamma$ . (a) At  $\hbar\omega_0 = 8\hbar\omega_R$ , the band minima of the lowest band is at  $M$  point. The band touching points are not accidental as they exist for a wide range of lattice depth. (b) The band degeneracy is broken in the presence of a Zeeman term ( $B = 0.1\hbar\omega_R$  used here).

terms into the same exponent.  $\hbar^2 k_{\text{so}}^2 (F_x^2 + F_y^2)/8m$  acts like a quadratic Zeeman shift. The leading order correction to the time evolution operator for the 2D ML is  $\delta U_{2D}^{(1)}(T, 0) \approx \max(\omega_0^2, \omega_R^2) \mathcal{O}(\delta t^2)$  assuming  $k_x, k_y \lesssim k_{\text{so}}$ , where  $\omega_R = \hbar k_{\text{so}}^2/2m$ . When the Trotter expansion fails, one can simply reduce free evolution time and build up the action through repeated pulse cycles [47]. More details can be found in the supplemental material. The synthesized  $\vec{B}(x, y) = B_0[-\sin(k_{\text{so}}y), \sin(k_{\text{so}}x), \cos(k_{\text{so}}x) + \cos(k_{\text{so}}y)]/2$  in our 2D ML  $H_{\text{eff}}^{(2D)}$  gives the following eigenvalues ( $|\vec{B}|, 0, -|\vec{B}|$ ), as shown in Fig. 2(a). Its typical band structure is shown in Fig. 3(a), which is similar to lattice models employed for p-orbital physics [49], and is different from usual OLs. The lowest two bands touch at  $\Gamma$  ( $K_x = 0, K_y = 0$ ) and  $X$  point ( $k_{\text{so}}/2, 0$ ) points. The third and fourth bands touch at  $M$  ( $k_{\text{so}}/2, k_{\text{so}}/2$ ) and  $X$  points. The band touching points are robust against tuning of lattice depth. The degeneracy can be broken leading to a gap if a Zeeman term ( $\propto BF_z$ ) is added to Eq. (3) as shown in Fig. 3(b).

Figure 4 compares a sampling of numerical simulations based on Gross-Pitaevskii equation. For a fixed

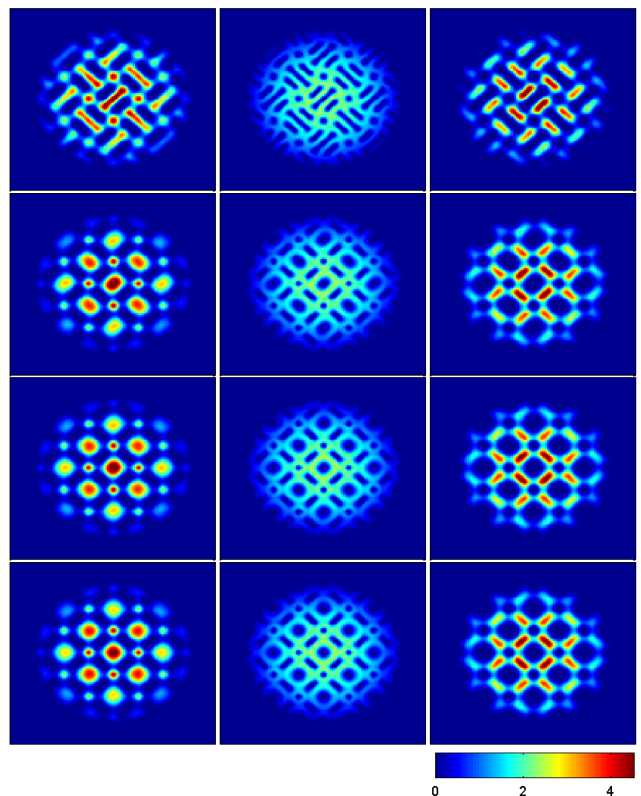


FIG. 4: The left, middle, and right columns respectively refer to atomic internal states  $|F = 1, M_F\rangle$  for  $^{87}\text{Rb}$  with  $M_F = 1, 0,$  and  $-1$ . Results from the actual dynamics are shown in the top 3 rows, going down respectively for  $\delta t = 50, 10,$  and  $2.5 \mu\text{s}$ . The last row comes from the effective dynamics.  $T = 100 \mu\text{s}$ ,  $B_0 = 10 \text{ mGauss}$  or  $\omega_0 = (2\pi)7.024 \text{ kHz}$ . The gradient pulses are the same with  $B' = 1000 \text{ Gauss/cm}$  and  $\delta t' = 1 \mu\text{s}$ , which gives  $k_{\text{so}} = 0.44 \mu\text{m}^{-1}$ , and  $\omega_R = (2\pi)11.23 \text{ Hz}$ . The regions displayed correspond to  $-15a_h < x, y < 15a_h$ , with  $a_h = \sqrt{\hbar/m\omega}$  the length scale for an isotropic harmonic oscillator  $\omega_x = \omega_y = \omega = (2\pi)30 \text{ Hz}$ .

evolution time  $T$ , actual dynamics are propagated using 1, 5, and 20 pulses as shown in the 1st, 2nd, and 3rd row respectively. With increasing numbers of pulse cycles, atomic density distributions converge towards that from the effective dynamics by  $H_{\text{eff}}^{(2D)}$ , which are shown in the last row. We find that the required error bounds  $\delta U_{2D}^{(1)}(T, 0) \leq \max(\omega_0^2, \omega_R^2)\delta t^2$  are always satisfied when  $\delta t$  becomes sufficiently short. Extensive simulations show that our idea is effective and efficient. This conclusion is also supported by the analytic derivation of the effective interaction above, where all approximations used are reasonable under most circumstances.

The ML we synthesize can be straightforwardly detected making use of lattice induced atomic diffractions as we illustrate in detail in the supplemental material for the 1D case. Both the SOC strength  $k_{\text{so}}$ , or the reciprocal vector of the ML, and the ML depth  $\hbar\omega_0$  can be independently tuned in our protocol. In the optical Raman scheme [40, 50],  $k_{\text{so}}$  is limited to two photon recoil

momentum. In our protocol, it is replaced by the momentum impulse from a single gradient pulse, provided the kinetic energy term during the gradient pulse can be neglected when  $\omega_R \delta t' \ll 1$ , (see supplemental material). To achieve  $k_{\text{so}} = 1(k_L) \sim 8 \mu\text{m}^{-1}$  (for a typical laser wavelength  $\lambda_L = 804 \text{ nm}$  [50]), the validity of our proposal requires  $\delta t' \ll 40 \mu\text{s}$  and  $B' \gg 427 \text{ Gauss/cm}$ . These conditions are already available in atom chip experiments with pulses as short as  $5 \mu\text{s}$  at a gradient of  $3.4 \text{ kGauss/cm}$  [51]. One can even go beyond  $k_{\text{so}} \sim k_L$ . For  $k_{\text{so}} = 4k_L \sim 32 \mu\text{m}^{-1}$ ,  $\delta t' \ll 2.5 \mu\text{s}$  is required if  $B' \gg 27.3 \text{ kGauss/cm}$  can be generated. Such a short and high gradient pulse is of course an experimental challenge. Nevertheless it is available in the state of art NMR experiments ( $1.4 \mu\text{s}$  and  $53.4 \text{ kGauss/cm}$ ) [52], and is perhaps also realizable with improved atom chips ( $0.5 \mu\text{s}$  and  $170 \text{ kGauss/cm}$ ) [51] using thin wires and tiny current loops. An unwelcomed drawback of using such high gradient magnetic field is due to quadratic Zeeman shift, which compromises energy level symmetry and reduces a spin  $F$  atomic system to a two-level or spin  $1/2$  system. It is interesting to point out that our protocol for synthesizing 1D ML can be alternatively viewed as a Ramsey like interferometer [53] with pulsed gradient magnetic fields acting as spatial dependent oscillating fields. The population oscillations discussed in the supplemental material are simply the interference signals. In this sense, our protocol for 1D ML also resembles the work of field gradient beam splitter (FGBS) [51].

The interaction terms  $\propto F_x, F_y$  of our ML couple spatial diffraction with atomic spin flips, thus it can also be viewed as a particular type of SOC. However, when reduced to 1D, the diffraction orders of our ML becomes finite, constrained by the finite spin, rather than being infinite as for the usual spin dependent lattices  $\propto F_z$ . When spin flip pulses or additional free evolution periods are introduced between successive 1D ML pulse pairs, the  $F_y$  terms can be compensated for. This will effectively reduce our ML in 1D to the usual  $\propto F_z$  type lattice with broken continuous translation symmetry, allowing for spatial diffraction to infinite orders. The 2D ML synthesized with our protocol always breaks continuous translation symmetry, thus is capable of infinite order spatial diffraction by itself. It encompasses the combined effects of a usual spin dependent lattice and SOC. Although the band structure we show earlier is topologically trivial, several variants of Eq. (3), generated by other pulse sequences, indeed display nontrivial topological band structure, which will be further explored and published elsewhere. To our knowledge, this type of 2D

ML has not been discussed in solid state materials.

Before conclusion, we discuss two experimental insights regarding the feasibility of realizing our ML protocol within the limits of current experimental capabilities. First, Our protocol makes use of gradient magnetic fields such as  $B'x\hat{x}$  to enact spatial dependent spin rotations. Such magnetic fields, however, cannot simply exist because the divergences and curls of magnetic fields vanish in free space. In actual experiments, the gradient field direction is slaved to the direction of the large bias field  $B_{x0}$ , as in selecting the  $x$ -gradient from the 3D quadruple field  $(B'x + B_{x0})\hat{x} + B'y\hat{y} - 2B'z\hat{z}$  [54]. One can also use a gradient RF magnetic field with a strong bias field to serve as gradient magnetic field [48]. Second, the  $x$ - ( $y$ -) direction gradient field pulses must be turned on and off abruptly as otherwise atomic spins will adiabatically follow the time dependent magnetic field. Experimentally the temporal rate of changing magnetic field is limited by the coil inductances and by eddy currents. Small coils boosted by high voltage power supplies can help produce rapid changing magnetic fields. The eddy current effects can be measured and compensated for by pre-emphasis current driving as widely employed in pulsed field gradients NMR experiments [55]. Instead of flipping the direction of the gradient magnetic field, we can alternatively flip the direction of atomic spin through rf coupling [56] or motion insensitive Raman transitions.

In conclusion, we propose an idea for generating a ML using pulsed gradient magnetic fields. The spatial dependent spin rotations from the gradient fields couple atomic internal states with its spatial motion, effectively synthesizing a ML. Both the lattice constant and its depth are tunable experimentally and can overcome the laser wavelength limit encountered in optical schemes. By applying  $x$ - and  $y$ -gradient fields successively and with sufficiently short free evolution times, the 1D ML protocol discussed above can be extended to realize a 2D ML. Atomic diffractions from the 1D ML give rise to population oscillations among spin-momentum states, which are easily observable and can falsify the synthesized ML. Finally, we discuss experimental approaches for implementing our protocols in today's cold atom experiments. The protocol we propose can be applied to both bosonic and fermionic atoms. The band structures of the synthetic ML display desirable features of interest to topological quantum matter research.

This work is supported by MOST 2013CB922002 and 2013CB922004 of the National Key Basic Research Program of China, and by NSFC (No. 91121005, No. 11274195, No. 11004116, and No. 11374176).

---

[1] I. Bloch, J. Dalibard, and W. Zwerger, Rev. Mod. Phys. **80**, 885 (2008).  
 [2] D. Jaksch and P. Zoller, Ann. Phys. **315**, 52 (2005).  
 [3] D. Jaksch, H. -J. Briegel, J. I. Cirac, C. W. Gardiner, and P. Zoller, Phys. Rev. Lett. **82**, 1975 (1999).

[4] G. K. Brennen, C. M. Caves, P. S. Jessen, and I. H. Deutsch, Phys. Rev. Lett. **82**, 1060 (1999).  
 [5] M. Karski, L. Foster, J. Choi, A. Steffen, W. Alt, D. Meschede, and A. Widera, Science, **325**, 174 (2009).  
 [6] M. Greiner, O. Mandel, T. Esslinger, T. W. Hansch, and

- I. Bloch, *Nature* **415**, 39 (2002).
- [7] L. Tarruell, D. Greif, T. Uehlinger, G. Jotzu, and T. Esslinger, *Nature* **483**, 302 (2012).
- [8] G. B. Jo, J. Guzman, C. K. Thomas, P. Hosur, A. Vishwanath, and D. M. Stamper-Kurn, *Phys. Rev. Lett.* **108**, 045305 (2012).
- [9] W. Han, S. Zhang, J. Jin, and W. M. Liu, *Phys. Rev. A* **85**, 043626 (2012).
- [10] D. C. McKay, C. Meldgin, D. Chen, and B. DeMarco, *Phys. Rev. Lett.* **111**, 063002 (2013).
- [11] J.-S. Bernier, K. Sengupta, and Y. B. Kim, *Phys. Rev. B* **74**, 155124 (2006).
- [12] O. Mandel, M. Greiner, A. Widera, T. Rom, T. W. Hansch, and I. Bloch, *Phys. Rev. Lett.* **91**, 010407 (2003).
- [13] P. J. Lee, M. Anderlini, B. L. Brown, J. Sebby-Strabley, W. D. Phillips, and J. V. Porto, *Phys. Rev. Lett.* **99**, 020402 (2007).
- [14] P. Soltan-Panahi, D. -S. Luhmann, J. Struck, P. Windpassinger, and K. Sengstock, *Nat. Phys.* **8**, 71 (2012).
- [15] A. Hubener, M. Snoek, and W. Hofstetter, *Phys. Rev. B* **80**, 245109 (2009).
- [16] I. Zapata, B. Wunsch, N. T. Zinner, and E. Demler, *Phys. Rev. Lett.* **105**, 095301 (2010).
- [17] S. R. Hassan, P. V. Sriluckshmy, S. K. Goyal, R. Shankar, and D. Senchal, *Phys. Rev. Lett.* **110**, 037201 (2013).
- [18] E. A. Ostrovskaya and Y. S. Kivshar, *Phys. Rev. Lett.* **92**, 180405 (2004).
- [19] G. Orso, E. Burovski, and T. Jolicoeur, *Phys. Rev. Lett.* **104**, 065301 (2010).
- [20] W. V. Liu, F. Wilczek, and P. Zoller, *Phys. Rev. A* **70**, 033603 (2004).
- [21] P. Soltan-Panahi, J. Struck, P. Hauke, A. Bick, W. Plenkers, G. Meineke, C. Becker, P. Windpassinger, M. Lewenstein, and K. Sengstock, *Nat. Phys.* **7**, 434 (2011).
- [22] J. Dalibard, F. Gerbier, G. Juzeliunas, and P. Ohberg, *Rev. Mod. Phys.* **83**, 1523 (2011), and references therein.
- [23] D. Jaksch and P. Zoller, *New J. Phys.* **5**, 56 (2003).
- [24] F. Gerbier and J. Dalibard, *New J. Phys.* **12**, 033007 (2010).
- [25] N. R. Cooper, *Phys. Rev. Lett.* **106**, 175301 (2011).
- [26] N. R. Cooper and J. Dalibard, *Eur. Phys. Lett.* **95**, 66004 (2011).
- [27] B. Beri and N. R. Cooper, *Phys. Rev. Lett.* **107**, 145301 (2011).
- [28] A. S. Sorensen, E. Demler, and M. D. Lukin, *Phys. Rev. Lett.* **94**, 086803 (2005).
- [29] T. Kitagawa, E. Berg, M. Rudner, and E. Demler, *Phys. Rev. B*, **82**, 235114 (2010).
- [30] K. Osterloh, M. Baig, L. Santos, P. Zoller, and M. Lewenstein, *Phys. Rev. Lett.* **95**, 010403 (2005).
- [31] M. Aidelsburger, M. Atala, M. Lohse, J. T. Barreiro, B. Paredes, and I. Bloch, *Phys. Rev. Lett.* **111**, 185301 (2013).
- [32] H. Miyake, G. A. Siviloglou, C. J. Kennedy, W. C. Burton, and W. Ketterle, *Phys. Rev. Lett.* **111**, 185302 (2013).
- [33] D. Cocks, P. P. Orth, S. Rachel, M. Buchhold, K. LeHur, and W. Hofstetter, *Phys. Rev. Lett.* **109**, 205303 (2012).
- [34] M. Gong, Y. Qian, V. W. Scarola, and C. Zhang, arXiv:1205.6211 (2012).
- [35] W. S. Cole, S. Zhang, A. Paramekanti, and N. Trivedi, *Phys. Rev. Lett.* **109**, 085302 (2012).
- [36] J. Radic, A. DiCiolo, K. Sun, and V. Galitski, *Phys. Rev. Lett.* **109**, 085303 (2012).
- [37] Z. Cai, X. Zhou, and C. Wu, *Phys. Rev. A* **85**, 061605(R) (2012).
- [38] G. Grynberga and C. Robilliard, *Phys. Rep.* **355**, 335 (2001).
- [39] J. Dalibard and C. Cohen-Tannoudji, *J. Opt. Soc. Am. B* **6**, 2023 (1989).
- [40] K. Jimenez-Garcia, L. J. LeBlanc, R. A. Williams, M. C. Beeler, A. R. Perry, and I. B. Spielman, *Phys. Rev. Lett.* **108**, 225303 (2012).
- [41] P. Windpassinger and K. Sengstock, *Rep. Prog. Phys.* **76**, 086401 (2013).
- [42] C. J. Kennedy, G. A. Siviloglou, H. Miyake, W. C. Burton, and W. Ketterle, arXiv:1308.6349 (2013).
- [43] L. W. Cheuk, A. T. Sommer, Z. Hadzibabic, T. Yefsah, W. S. Bakr, and M. W. Zwierlein, *Phys. Rev. Lett.* **109**, 095302 (2012).
- [44] J. Fortágh and C. Zimmermann, *Rev. Mod. Phys.* **79**, 235 (2007).
- [45] M. Singh, M. Volk, A. Akulshin, A. Sidorov, R. McLean, and P. Hannaford, *J. Phys. B: At. Mol. Opt. Phys.* **41**, 065301 (2008).
- [46] S. Whitlock, R. Gerritsma, T. Fernholz, and R. J. C. Spreeuw, *New J. Phys.* **11**, 023021 (2009).
- [47] Z. F. Xu, L. You, and M. Ueda, *Phys. Rev. A* **87**, 063634 (2013).
- [48] B. M. Anderson, I. B. Spielman, and G. Juzeliunas, *Phys. Rev. Lett.* **111**, 125301 (2013).
- [49] W. V. Liu and Congjun Wu, *Phys. Rev. A* **74**, 013607 (2006); G. Wirth, M. Olschlager, and A. Hemmerich, *Nat. Phys.*, **7**, 147 (2011).
- [50] Y.-J. Lin, K. Jimenez-Garcia, and I. B. Spielman, *Nat. Lett.* **471**, 83 (2011).
- [51] S. Machluf, Y. Japha, and R. Folman, *Nat. Commun.* **4**, 2424 (2013).
- [52] L. Shtirberg, Y. Twig, E. Dikarov, R. Halevy, M. Levit, and A. Blanka, *Rev. Sci. Instrum.* **82**, 043708 (2011).
- [53] N. F. Ramsey, *Phys. Rev.* **78**, 695 (1950).
- [54] H. J. Metcalf and W. D. Phillips, *Metrologia*, **22**, 271 (1986).
- [55] J. J. V. Vaals and A. H. Bergman, *J. Magn. Reson.*(1969) **90**, 52 (1990).
- [56] E. L. Hahn, *Phys. Rev.* **80**, 580 (1950).

# Supplementary material: generating an effective magnetic lattice for cold atoms

Xinyu Luo,<sup>1,2,3</sup> Lingna Wu,<sup>1,3</sup> Jiyao Chen,<sup>1,3</sup> Rong Lu,<sup>1,3</sup> Ruquan Wang,<sup>2,3</sup> and Li You<sup>1,3</sup>

<sup>1</sup>*State Key Laboratory of Low Dimensional Quantum Physics,  
Department of Physics, Tsinghua University, Beijing 100084, China*  
<sup>2</sup>*Institute of Physics, Chinese Academy of Sciences, Beijing 100080, China*  
<sup>3</sup>*Collaborative Innovation Center of Quantum Matter, Beijing, China*

(Dated: October 8, 2018)

PACS numbers: 67.85.Jk, 03.75.Mn, 03.75.Ss, 37.10.Jk

## I. THE VALIDITY CONDITIONS FOR THE EFFECTIVE HAMILTONIAN

In the main text, the effective two dimensional magnetic lattice Hamiltonian is derived by employing two approximations. First, the Zeeman term  $k_{\text{so}}x F_x$  is assumed to overwhelm all other interactions during the gradient magnetic field pulse, and second, higher order terms are neglected when non-commuting exponents  $A$  and  $B$  are combined into the same exponent according to  $e^{A\delta t}e^{B\delta t} \simeq e^{(A+B)\delta t}$ . This section provides the validity conditions for these two approximations by making use of the Trotter expansion to the first order,

$$e^{A\delta t}e^{B\delta t} \simeq e^{(A+B)\delta t}e^{[A,B]\delta t^2/2}. \quad (1)$$

### A. The condition for neglecting atomic motion during the gradient pulse

Taking into account the atomic motion during the gradient magnetic pulse, the lowest order Trotter expansion for the single gradient pulse evolution operator is found to be

$$\begin{aligned} \bar{U}_x(\delta t') &= \exp \left\{ ik_{\text{so}}x F_x - i \frac{\hbar k_x^2}{2m} \delta t' \right\} \\ &\approx \exp \left\{ i \frac{\hbar k_{\text{so}}}{2m} k_x F_x \delta t' \right\} \exp \left\{ -i \frac{\hbar k_x^2}{2m} \delta t' \right\} \exp \{ ik_{\text{so}}x F_x \} \\ &= \exp \{ i\omega_R \delta t' (k_x/k_{\text{so}}) F_x \} \exp \left\{ -i\omega_R \delta t' (k_x/k_{\text{so}})^2 \right\} \exp \{ ik_{\text{so}}x F_x \}. \end{aligned} \quad (2)$$

The last factor is the spatial dependent spin rotation discussed in the main text, while the deviations of the first two multiplying from unity accounts for the error due to the neglect of atomic motion during the gradient magnetic field pulse. The first factor denotes an ‘extra’ spin rotation caused by atomic motion, which can be safely neglected provided

$$\omega_R \delta t' \ll 1, \quad (3)$$

assuming  $k_x, k_y \lesssim k_{\text{so}}$ . For ultracold atoms at tens or hundreds of nK considered in this study,  $k_x, k_y \lesssim k_{\text{so}}$  is always satisfied as it is simply equal to the statement of well below the recoil limit temperature, if we take a more typical momentum impulse of  $k_{\text{so}} = 1$  ( $k_L$ ). The neglect of atomic motion during the gradient pulse can be well satisfied as we illustrate in Fig. S1, which compares density distributions from the effective Hamiltonian (in the first column) with that from the dynamics of the discussed pulse sequence  $\omega_R \delta t' = 0.01, 0.1, \text{ and } 1$  (in the 2nd, 3rd, and 4th column, from left to right). We see as  $\omega_R \delta t'$  becomes smaller, the approximation becomes better, and the atomic density distributions uniformly converge towards that from the effective dynamics.

### B. The condition for achieving the 2D magnetic lattice

We now proceed to investigate the condition for the second approximation. According to our protocol developed in the main text, we set

$$\begin{aligned} A &= \frac{\hbar}{2m} \left[ (k_x - k_{\text{so}} F_x)^2 + k_y^2 \right] + \omega_0 [F_z \cos(k_{\text{so}}x) + F_y \sin(k_{\text{so}}x)], \\ B &= \frac{\hbar}{2m} \left[ (k_y - k_{\text{so}} F_y)^2 + k_x^2 \right] + \omega_0 [F_z \cos(k_{\text{so}}y) - F_x \sin(k_{\text{so}}y)], \end{aligned} \quad (4)$$

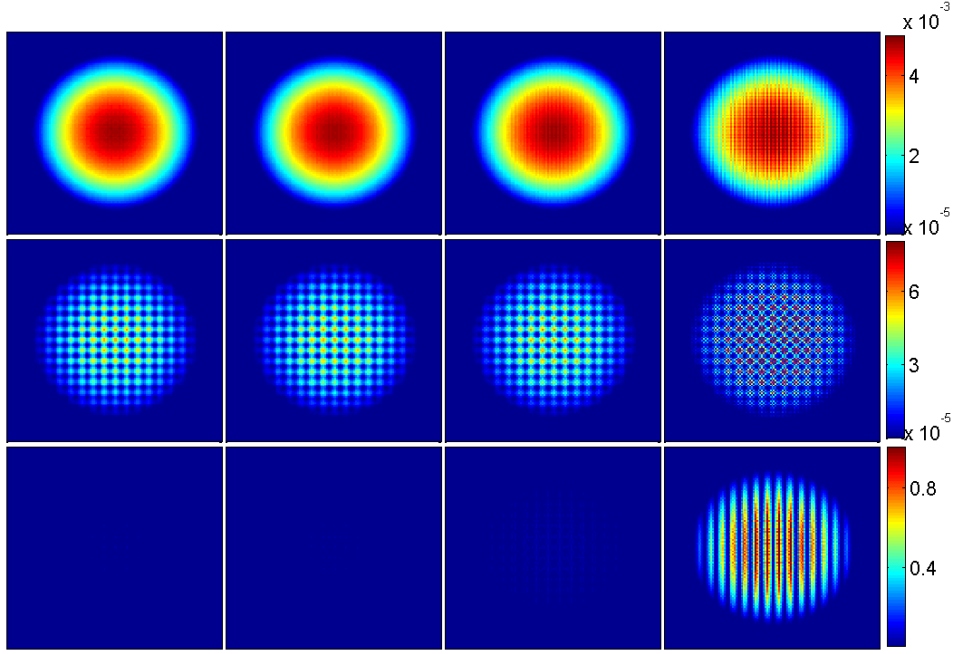


FIG. S1: Atomic density distributions from the effective Hamiltonian dynamics (in the first column) are compared with results from the actual pulse sequence shown in the 2nd, 3rd, 4th columns, respectively for  $\omega_R \delta t' = 0.01, 0.1,$  and  $1$ . From top to down, the three rows respectively show atomic densities in internal state  $|F = 1, M_F\rangle$  for  $^{87}\text{Rb}$  with  $M_F = 1, 0,$  and  $-1$ . The parameters used give the same momentum impulse  $k_{\text{so}} = 1k_L \sim 7.8 \mu\text{m}^{-1}$ , (for a typical laser wavelength  $\lambda_L = 804\text{nm}$ ). Other parameters are as discussed in the main text:  $\delta t = 2.5 \mu\text{s}$ ,  $B_0 = 10 \text{ mGauss}$  or  $\omega_0 = (2\pi)7.024 \text{ kHz}$ . The regions displayed correspond to  $-15a_h < x, y < 15a_h$ , with  $a_h = \sqrt{\hbar/m\omega}$ , the length scale for an isotropic harmonic oscillator  $\omega_x = \omega_y = \omega = (2\pi)30 \text{ Hz}$ .

the commutator between  $A$  and  $B$  is found to be

$$\begin{aligned}
[A, B] = & i\omega_R^2 \{(k_x/k_{\text{so}} - F_x), \{(k_y/k_{\text{so}} - F_y), F_z\}\} + \\
& i\omega_R\omega_0 [\{(k_x/k_{\text{so}} - F_x), F_y\} \cos(ky) + \{k_y/k_{\text{so}}, F_z \sin(k_{\text{so}}y) + F_x \cos(k_{\text{so}}y)\}] + \\
& i\omega_R\omega_0 [\{(k_y/k_{\text{so}} - F_y), F_x\} \cos(kx) - \{k_x/k_{\text{so}}, F_z \sin(k_{\text{so}}x) - F_y \cos(k_{\text{so}}x)\}] + \\
& i\omega_0^2 [F_x \sin(k_{\text{so}}x) \cos(k_{\text{so}}y) - F_y \cos(k_{\text{so}}x) \sin(k_{\text{so}}y) + F_z \sin(k_{\text{so}}x) \sin(k_{\text{so}}y)], \quad (5)
\end{aligned}$$

where  $\omega_R = \hbar k_{\text{so}}^2/2m$ , and  $\{F_i, F_j\} = F_i F_j + F_j F_i$  denotes anticommutator. For spin-1/2 particles,  $F_j = \sigma_j$ , which gives  $\{F_i, F_j\} = 0$  if  $i \neq j$ . Equation (5) in the above reduces to

$$\begin{aligned}
[A, B] = & i\omega_R^2 \frac{2k_x k_y}{k_{\text{so}}^2} \sigma_z + \\
& i \frac{\omega_R \omega_0}{2k_{\text{so}}} [\{k_y, \cos(k_{\text{so}}x) + \cos(k_{\text{so}}y)\} \sigma_x] + \\
& i \frac{\omega_R \omega_0}{2k_{\text{so}}} [\{k_x, \cos(k_{\text{so}}x) + \cos(k_{\text{so}}y)\} \sigma_y + (\{k_y, \sin(k_{\text{so}}y)\} - \{k_x, \sin(k_{\text{so}}x)\}) \sigma_z] + \\
& i \frac{\omega_0^2}{2} [\sigma_x \sin(k_{\text{so}}x) \cos(k_{\text{so}}y) - \sigma_y \cos(k_{\text{so}}x) \sin(k_{\text{so}}y) + \sigma_z \sin(k_{\text{so}}x) \sin(k_{\text{so}}y)]. \quad (6)
\end{aligned}$$

The leading order correction to the time evolution operator for the 2D ML is therefore  $\delta U_{2D}^{(1)}(T, 0) \approx \max(\omega_0^2, \omega_R^2) O(\delta t^2)$ . The condition for combining the otherwise non-commuting  $x$ - and  $y$ -dependent exponents to forming the 2D ML in the same exponent is then simply given by

$$\max(\omega_0^2, \omega_R^2) \delta t^2 \ll 1, \quad (7)$$

which is supported by Fig. 4 in the main text.

## II. DETECTION OF MAGNETIC LATTICE

A ML induces atomic diffraction, which in turn can be used for its detection. We illustrate below for the 1D case. In the parameter regime discussed here,  $\omega_0 \gg \omega_R$ , the Hamiltonian  $H_{\text{eff}}^{(x)}$  [Eq. (2) of the main text] then reduces to

$$H_x = \hbar\omega_0 [F_z \cos(k_{\text{so}}x) + F_y \sin(k_{\text{so}}x)], \quad (8)$$

after neglecting the SOC term. It is invariant under continuous spatial translation along  $x$ -direction. After a  $\pi/2$  spin rotation transformation about the  $y$ -axis, it becomes

$$\begin{aligned} H'_x &= e^{-i\frac{\pi}{2}F_y} H_x e^{i\frac{\pi}{2}F_y} \\ &= \frac{1}{2}\hbar\omega_0 (F_+ e^{-ik_{\text{so}}x} + F_- e^{ik_{\text{so}}x}), \end{aligned} \quad (9)$$

where  $F_{\pm} = F_x \pm iF_y$  are the spin raising and lowering operators. Thus the ML  $H_x$  represents a particular type of SOC, as an atom lowers (raises) its internal spin state, it gains (or loses) momentum  $\hbar k_{\text{so}}$ . If the ML is suddenly turned on, atoms will start to oscillate among different spin-momentum eigenstates  $|M_F, k_x = nk_{\text{so}} + k_x^{(0)}\rangle$  with frequency  $\omega_0$ , similar to the Raman coupled SOC scheme.  $k_x^{(0)}$  denotes the initial atomic kinetic momentum. The spin-momentum population oscillation can be detected by time of flight Stern-Gerlach imaging, which gives a clear signature of the synthesized 1D ML, as illustrated in Fig. S2.

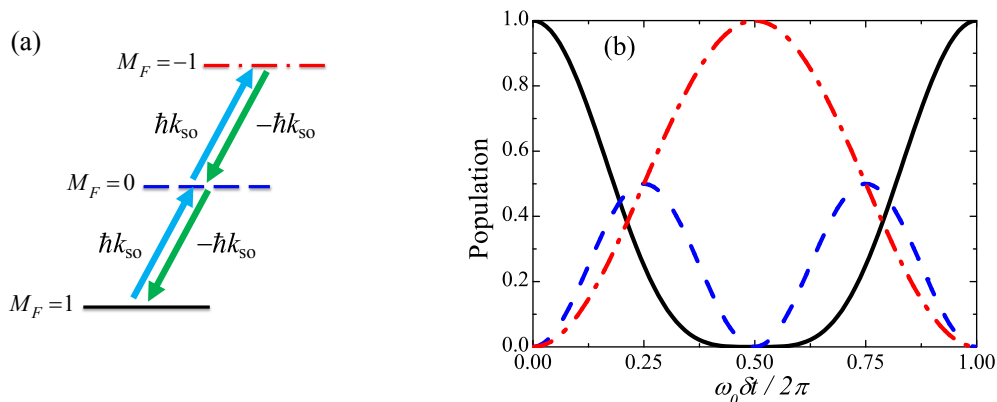


FIG. S2: (a) The ML couples different spin-momentum states  $|M_F, k_x = nk_{\text{so}}\rangle$ . Atoms gain (or lose) momentum  $\hbar k_{\text{so}}$  when their internal spin states are lowered (raised). (b) Oscillating populations. The red dot-dashed, blue dashed, and black solid lines respectively correspond to states  $|M_F = -1, n = 2\rangle$ ,  $|M_F = 0, n = 1\rangle$ , and  $|M_F = 1, n = 0\rangle$ .